Chapter 9

Trench Filling by Physical Vapor Deposition

9.1 Introduction

The manufacture of semiconductor integrated circuits requires hundreds of steps from production of the silicon wafers through final testing of a packaged component [1]. The formation of metal interconnections is a key aspect in the process. The general trend in the area is away from blanket coatings and subsequent reactive ion etching patterning towards damascene processes, which utilize the filling of embedded trenches and vias and subsequent planarization by chemical-mechanical polishing. The width dimension (less than half micron) and aspect ratios (i.e. depth:width > 1) of these trenches and vias are generally incompatible with conventional sputter deposition due to the broad angular distribution of the sputtered atoms [16]. Sputter deposition into these features results in overhang and eventual void formation, which causes increased resistance and reliability concerns. Three solutions to this problem established over the years have been ionized PVD [1], CVD [150] and electroplating [151]. CVD by surface reaction kinetics is advantageous for deposition in high aspect ratio cases, but it has problems such as low deposition rate, poor reproducibility, poor polycrystalline texture control, and contamination, etc. [152]. The emerging electroplating process has better filling capability for high aspect ratio features than sputtering or CVD and is projecting to play major role in future microelectronics industry, although it needs a seed layer to guide film growth and a barrier layer to prevent conducting metal from reaching and destroying active devices. The seed and barrier layer (collectively called liner layer) are both prepared by ionized PVD. Alterna-

tively, ionized PVD in combination with reflow is considered to be a key technology in ULSI manufacturing especially for via holes of higher level interconnects whose aspect ratio is not very large [152].

This chapter addresses the important PVD process. The evolution of PVD technology in metallization and previous simulations in the area are first described, followed by modeling work.

9.2 PVD metallization

9.2.1 Metallization experiments

PVD in the microelectronics industry generally refers to sputter deposition. There are a number of reasons why PVD sputter has been so successful in the field [12]. First, sputtering can be used to deposit all of the conducting films used in interconnect metallization schemes, including metals with vastly different melting points such as aluminum (T_m = 660°C) and titanium (T_m = 1670°C). Second, deposition of alloys can be accomplished from a single alloy target with the film retaining the stoichiometry. This is problematic with evaporation due to different individual vapor pressures. Third, the deposition rate can reach 1 µm/min for thick films, sufficient for economical wafer fabrication [12]. Fourth, sputter films have superior purity, microstructure and surface roughness for physical and process requirements. Finally, the use of an extended target area minimizes spatial variations of film thickness and shadowing which results in good step coverage over features provided aspect ratio < 1 [12]. As a result, ever since PVD emerged in the 1970s as a production-worthy technology for microelectronic fabrication, its major application has continued to be metallization and interconnection [12].

The isotropic nature of the sputtered atoms, valuable for coherently coating over steps, edges and other low aspect ratio surface features, creates a problem for deposition into high aspect ratio features such as those used in a damascene process. The majority of

the depositing atoms are moving at angles far from normal incidence, which results in significant lateral deposition on the upper sidewalls. Such lateral build-up quickly results in a narrowing and eventual closure of the trench or via. Since sputtered atoms are primarily neutral, their trajectory cannot be controlled by electric fields.

A variety of approaches have emerged to improve its usability for high aspect ratio features in the course of microelectronics applications. They can be divided into two groups: those based on the deposition of neutral species, and those based on the deposition of ions. The former includes the geometrical filtering of the sputtered flux [16] and increase of the surface mobility of the deposited atoms on the wafer surface [16]. The latter controls incidence directionality by using in-flight ionization of a sputtered or evaporated flux together with acceleration of the metal ions to the sample using a bias voltage. In such case, resputtering and grazing angle ion bombardment can then be induced.

Flux collimation belongs to the directional filtering [14, 15]. Often using spot welded sheetmetal arrays of hexagonal holes, the efficiency of the collimator depends on the aspect ratio of the collimators holes. Larger collimator aspect ratio results in more filtering, but an accompanying lower deposition rate, more frequent clogging, particle formation and costly maintenance. Because of the low efficiency and handling inconvenience, collimation is often limited to the deposition of the thin (diffusion inhibiting) liner coating. It is rarely used for filling a trench or via. [1].

Long-throw deposition is another geometrical filtering. By moving the sample farther away from the target, an increasing fraction of the sputtered atoms which are moving mostly laterally are lost to the chamber walls. This practice requires low chamber pressure to reduce in-flight gas scattering. It also introduces a fundamental geometrical asymmetry because the incidence angle distribution at the substrate edge is intrinsically different from that at the center. Because of the long distance, the deposition rate is also low.

On the other hand, the thermal reflow attempts to make use of the conducting metal's temperature-dependent surface property [19]. The argument is that if surface atoms have sufficient mobility, they may migrate down into deep features, resulting in enhanced filling. Thus the initial incidence directionality becomes unimportant. There are a number of requirements for any successful reflow process. First, the feature must remain open in the course such that there is a continuous surface from the field region to the bottom of the feature. Secondly, an adhesion layer must be first deposited to prevent agglomeration. Third, reflow requires high levels of cleanliness as contamination significantly impede the mobility of the surface atoms [1]. Although reflow have been successfully applied to the AlCu and copper interconnect systems, those requirements especially the open throat limits both the sputter deposition rate as well as the smallest feature size. A related technique is force-fill, which is more complicated [153].

The methods that have the potential to extend the PVD technology several chip generations are typified by ionized PVD (I-PVD) which is based on in-flight ionization of a sputtered or evaporated flux and the subsequent acceleration of the metal ions to the sample by means of an electrical potential [1]. This technique was first applied to the deposition of copper on semiconductor features by Holber *et al*. [154] who evaporated copper into an electron cyclotron resonance (ECR) plasma, and then condensed films from copper ions on a nearby, negatively biased wafer. More recently, deposition with metal ions has been extended to a related technology using magnetron sputtering as the metal source and inductively coupled RF plasmas as the means of ionization [1]. This latter technique has the advantage of compatibility with existing manufacturing hardware and processes as well as the capability to deposit alloys.

In I-PVD, metal atoms are sputtered from a conventional magnetron source using an inert gas and a conventional magnetron power supply. A second plasma, nominally different from the magnetron source plasma, is produced in the region between the sputtering

source and the sample using the same background gas. Some fraction of the sputtered metal atoms are ionized as they transit this second plasma. Finally, just above the sample surface, the metal ions are accelerated to the sample by the difference between the plasma potential (usually slightly positive) and the sample potential, which can be controlled externally to be either a zero or a negative voltage.

The transition from a conventional PVD process to the I-PVD concept took more than a decade of trial and error search in the laboratory and then the scaled up for the production line. Many of the intermediate explorations, consuming significant amount of research and development time, are short lived either because of complexity or because of low throughput and poor efficiency.

Today, the microelectronics industry is faced with the economic and technical challenge of making ultralarge scale integrated devices having minimum feature size 0.18 µm [16, 155]. Additional challenges are posed by the increase in silicon wafer size from 200 mm to 300 mm, the replacement of Al alloy interconnects with copper interconnects, and the related requirements for high quality copper diffusion barrier films and damascene processing. In order to meet the metallization challenge of ULSI devices, processes for metallization need to be explored and optimized with a minimum of experiments. This naturally leads to the question: whether or not many of those intermediate steps can be waived by using some type of predictive modeling, such as atomistic simulations; and whether or not the most rewarding route can be indicated by modeling. This chapter attempts to simulate the atom by atom assembly of trench metallization processes using the energy-dependent kMC method developed earlier. It addresses major process parameters including substrate temperature, deposition rate, adatom kinetic energy, the flux distribution and the trench geometry.

9.2.2 Metallization simulations

Various tools simulating PVD deposition have been developed by the microelec-

tronics community. They can be roughly divided into two categories; continuum-based methods and those based on atomistic models. The continuum approach seeks to represent the surface by a sequence of nodes and strings such as in the SHADE method [156], the SAMPLE method [157], and the SPEEDIE method [158] or described by an equation with mesh points (or cells) embedded in the system such as in the emerging level set method of Sethian [159]. The basic idea is to first numerically calculate the speed with which the material is to be added to or removed from a node (or a cell) which depends on the net effect of deposition, etching and other processes. An algorithm (e.g. shock wave [156]) is then used for incremental surface advancement. To approximate the effects of the impacting atoms kinetic energy, a sticking coefficient approximation is sometimes made. The angular distribution of the incident flux can also be incorporated. Important factors such as self-flux shadowing by protuberances on the surface have sometimes been included [156], enabling the topography of the growth surface to be evolved in a metallization process. However, the often considerable effect of temperature and deposition rate can not be sensibly simulated by these methods yet because of the difficulty of incorporating diffusion both on and beneath the growth surface. Although a continuum method is likely to be the eventual approach for a large wafer scale assessment, it is currently unsuited to the analysis of individual device features that have entered the deep sub-micron (<0.2 µm) region where diffusion distances can be compared to the dimensions of the feature.

Current atomistic approaches for simulating metallization usually are based on the SIMBAD method, a Monte Carlo model [160]. In this approach, the effect of temperature or deposition rate, surface diffusion is usually approximated by a "mobility" factor. A landed adatom or a disk is allowed to move a specified distance once before stopping for good. A higher temperature is modeled by a longer distance. The effects of adatom kinetic energy (reflection and resputtering) were treated using data from experimental measurements. Often the data for a specific metal under certain conditions are rarely available and approximations have to be made to fit needed conditions. This type of model then is sup-

posed to be able to simulate process conditions. However, since diffusion of any one of the atoms in the system is once allowed, the constant rearrangement of the whole atomic configuration can not be simulated, and since time is also not explicitly included, the role of the deposition rate can not be quantitatively analyzed nor its trade-off against temperature.

The latest attempt in simulating interconnect metallization was conducted by Huang, Gilmer and de la Rubia [54]. Their kMC approach was able to simulate the effect of substrate temperature and deposition rate but did not included the role of kinetic energy. Therefore, the model can only address low energy deposition; processes such as I-PVD are not appropriate.

9.3 Methodology

To simulate the I-PVD metallization processes, two major steps need to be addressed. The primary one is to properly treat the atomic diffusion. When deposition takes place in zone I and/or zone II of the structure zone model [45], it is the surface diffusion that dominates the evolution of surface profile while the bulk diffusion is negligible. An appropriate diffusion model thus is the critical element to simulate the growth process. It should reflect the dynamic nature of constant rearrangement of the entire simulation system, i.e. any one of the atoms in the system should be allowed to move at any time in the whole simulation process as long as it has the probability to do so. In this regard, the kMC method presented in chapter three is the best solution so far. The second step is to incorporate the interactions of energetic incident atoms with the growing film. This includes the reflection, resputtering, biased diffusion and athermal rearrangement caused by thermal spike. A schematic drawing for such effects is shown in Fig. 9.1. In this respect, the treatment used in chapter eight is equally suitable for a featured substrate. The methodology described in chapter eight was therefore employed here.

**ENERGY-DEPENDENT
ADATOM-SUBSTRATE INTERACTIONS**
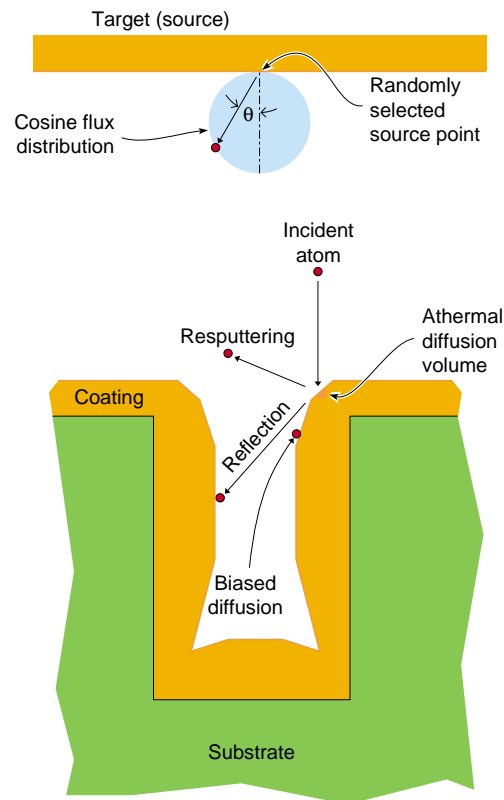
Fig. 9.1. Schematic geometry of interactions of an energetic incident atom with a trench. The incidence angle of the atoms are assumed to be represented by a cosine probability distribution. All major interaction events are indicated including reflection, resputtering, biased diffusion and athermal diffusion.

Different PVD processes often have different metal flux distributions at the substrate. The introduction of incident fluxes in a PVD process simulation is therefore worthy explanation. The angular distribution of sputtered atoms is generally described as a cosine distribution, Fig. 9.2(a) [26]. That is, the relative fluxes in each direction can be represented by the fluxes at the normal direction times the cosine of the angle from the surface normal. The angular distributions of collimated incidence and long-throw deposition can be represented by Fig. 9.2(b) [16]. The magnitude of θ is determined either by aspect ratio in case of collimator or by the distance between the cathode and the substrate in case of long-throw. The bigger the aspect ratio or the longer the distance, the smaller the θ. In I-

PVD, the ions are concentrated near $\theta = 0°$, whereas the neutral species follow a cosine-like distribution. Thus the overall distribution can be viewed as a superposition of a cosine and directional distribution, Fig. 9.2(c). The relative magnitude of the two components depends on the ionization ratio. High levels of ionization of the metal species are possible (e.g. > 75%), and in this case the majority of the depositing species arrive at normal incidence to the sample surface when a bias voltage is applied.

Experience has shown that filling larger aspect ratio features needs very directional flux so that it reaches the bottom of the feature without shadowing from the sidewalls. Such directionality can only be achieved by applying a pull upon incident atoms using bias voltage (about 20 eV at least [156]) on substrate. However, to deposit a liner layer, a more divergent incidence is desired to cover both the bottom and the sidewalls.
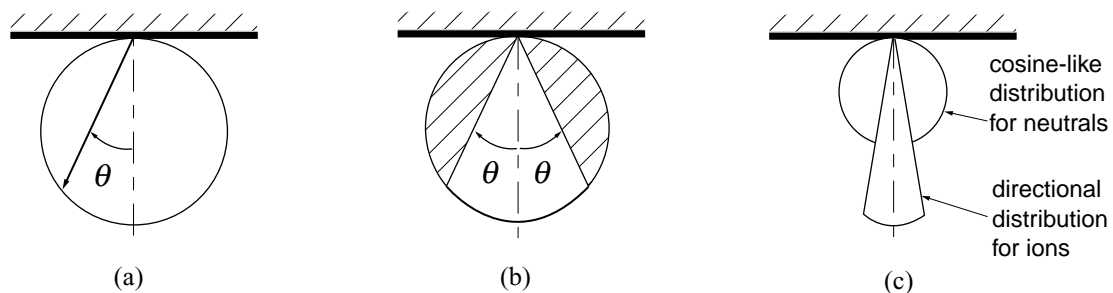
Fig. 9.2. Representative incidence distributions in PVD deposition. (a) conventional cosine distribution, (b) collimated distribution, and (c) distribution in I-PVD process where the circle represents neutral atoms' and the sector the ions' distribution.

9.4 Trench filling Results

The simulation methodology developed in chapter seven has been used to investigate the filling of trenches under various conditions. To quantify filling performance a filling factor has been calculated. It was defined as the ratio of the number of occupied lattice sites in a trench to the total number of available sites. The advantage over more traditional definitions of step coverage (e.g. the ratio of film thickness inside the feature to that out-

side the feature) is that the filling factor is a direct measurement of the status of the filling performance and is simple to calculate after (or during) a simulation. Periodic boundary conditions were used to avoid the effects of a limited system size. A total of 80,000 nickel atoms were used for each simulation. A typical run took about four hours of CPU time on a RS/6000 workstation. To minimize the statistical data spread, five runs were conducted and the average was used for each data point.

9.4.1 Effect of incident collimation

Fig. 9.3 shows the effect of incident collimation on the surface morphology. The deposition was conducted at a substrate temperature of $T/T_m = 0.48$ K, a deposition rate of 1.0 µm/min, a kinetic energy of 50 eV and trench aspect ratio of 2. It shows that best filling was achieved with a cut-off of ±3° (or less). However, complete filling was still achievable for a cut-off of ±11°. Increasing the angle of incidence to ±16° resulted in void formation. Apparently, complete filling prefers more a restrict cut-off.

To fully explore the collimation effect, more simulations at similar conditions have been conducted and the results are shown in Fig. 9.4. Here, 13 cut-off angles were used and the filling factor was calculated four times at different filling stages. The results surprisingly indicate the existence of a maximum filling efficiency at about 5°. The peak is initially unclear and becomes evident with the process. Intuitively, this means that the sum of atoms directly getting into the inside of the trench and those reflected and/or resputtered into the inside of the trench reach a maximum at certain collimation angle. The fraction that directly reach the trench bottom decreases with increasing the angle, while the reflected/resputtered fraction increases with increasing the angle. The two components work against each other and reach a maximum at a nonzero cut-off. At larger cut-off angles, more reflected and resputtered atoms redeposit at the trench throat area and result in a pinch-off.
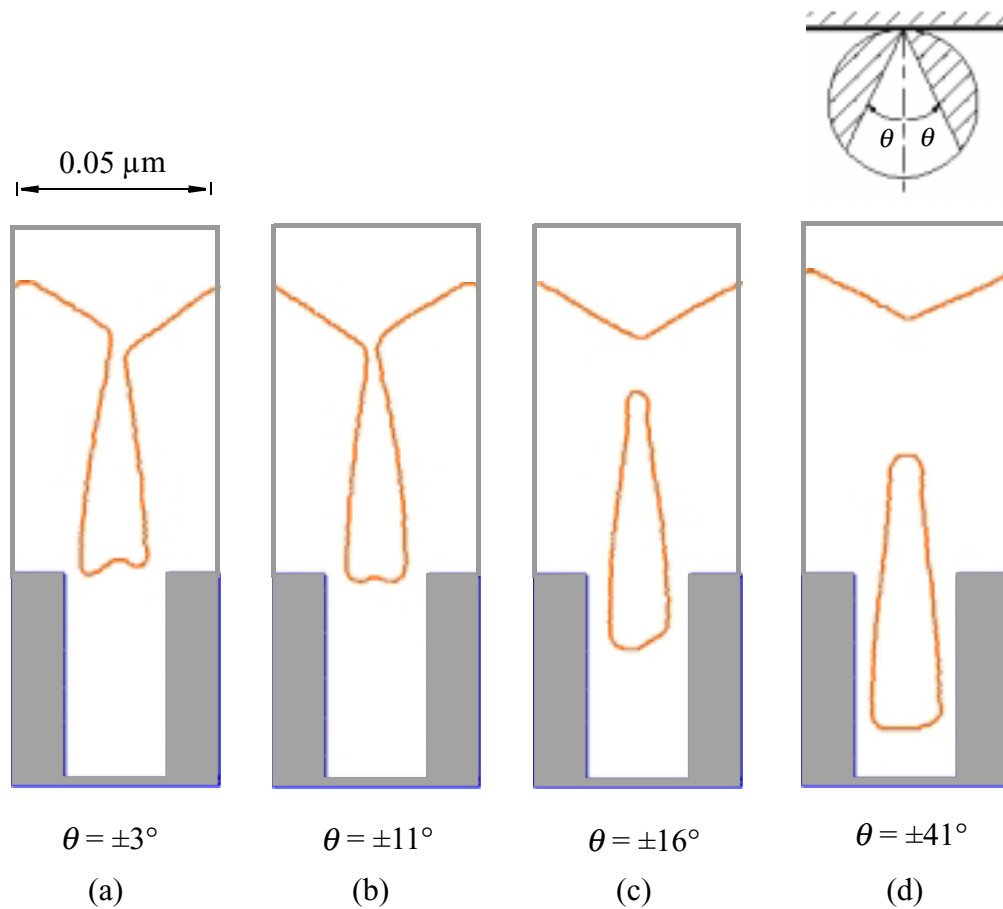
Fig. 9.3. Effect of incidence collimation angle on trench filling. The substrate temperature was 550 K (T/T_m = 0.48), the kinetic energy 50 eV, the deposition rate 1.0 μm/min and the aspect ratio of 2. Nickel atoms of 80000 were used in the simulations.
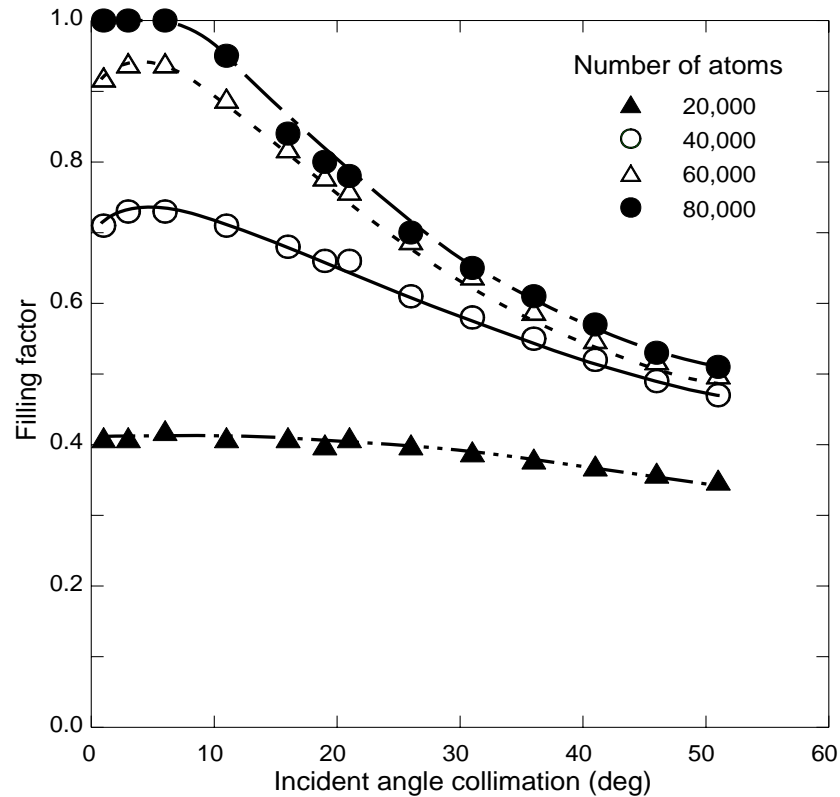
Fig. 9.4. Effect of incidence collimation angle on filling factor. The substrate temperature $T = 550$ K ($T/T_m = 0.48$), the deposition rate was 1.0 µm/min, the kinetic energy 50 eV and the aspect ratio of 2. The symbols serve to show the effect of deposition stage on filling factor.

The curves also expose big differences for the filling efficiency at various stages. At $n = 20,000$, the filling factor decreases slightly with increasing θ. At 40,000 and more, it decreases much faster. When fixing θ, the filling efficiency depends greatly on the number of deposited atoms. At 10°, for example, it takes 20,000 atoms to achieve a filling factor of 40%, 40,000 to about 72%, 60,000 to 89% and 80,000 to 97%. These dependences result from both a changing aspect ratio in the deposition and the formation of overhangs.

9.4.2 Effect of incident energy

Fig. 9.5 shows the effect of incident energy on trench filling. A cut-off angle of 11° and conditions otherwise identical to Fig. 9.3 were used. At a low energy of 10 eV, a
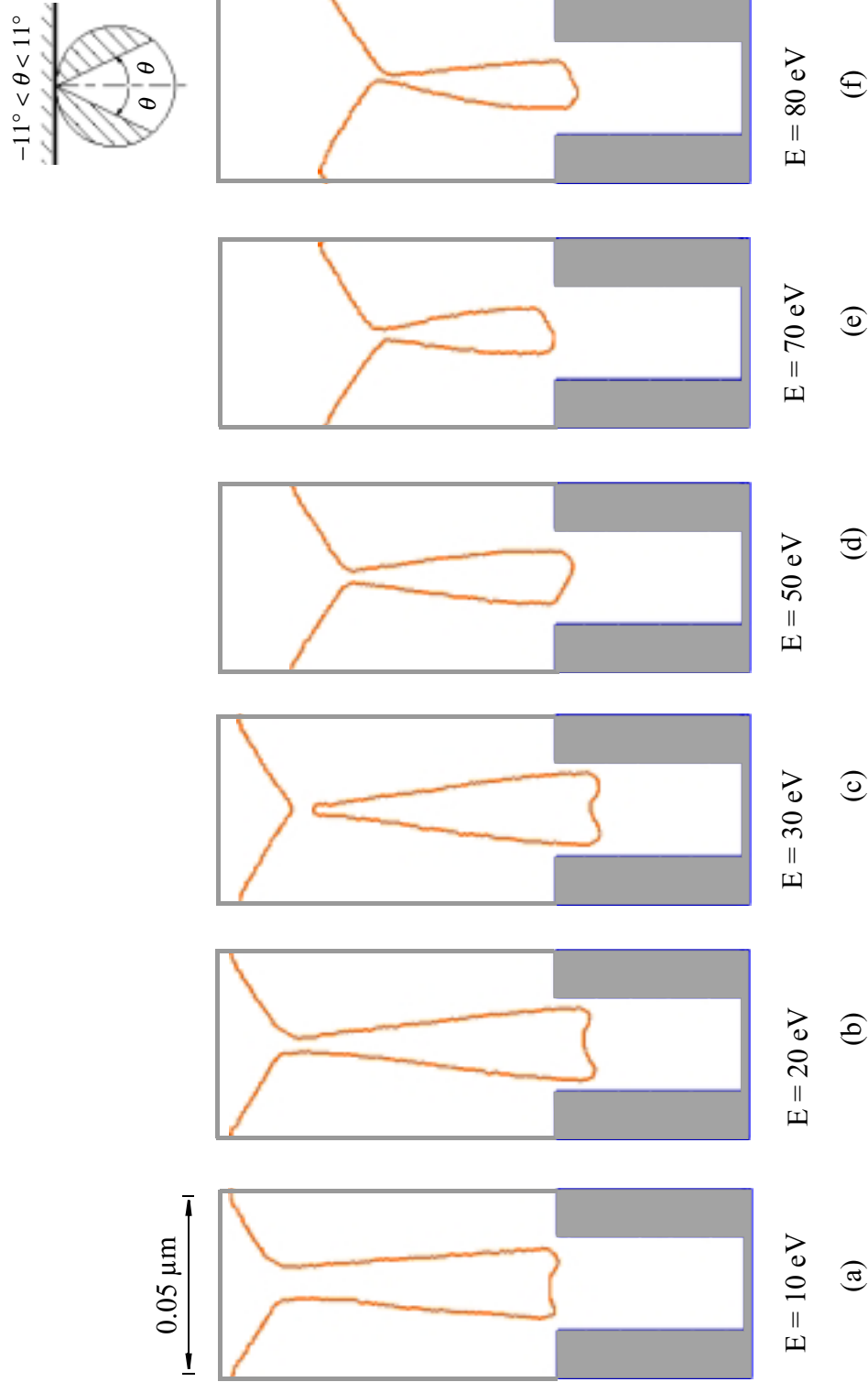
Fig. 9.5. Effect of incidence energy on trench filling. The substrate temperature was 550 K ($T/T_m = 0.48$), the incident collimation angle 11°, the deposition rate 1.0 μm/min and the aspect ratio of 2. Nickel atoms of 80000 were used in the simulations.

complete fill is seen. The wide opening at the top indicates no immediate risk of pinch-off. At 20 eV, the filling becomes worse and the opening at the top is reduced. When the energy is increased to 30 eV, filling deteriorated to point where a pinch-off had formed. However, the trend was reversed at 50 eV with the pinch-off gone and the filling improved. The new trend continued to an energy of 70 eV where a complete fill was reached. With further increase of energy, the filling decreased again. The detailed trend of energy dependence of trench filling can be best seen in Fig. 9.6. Fig. 9.6 indicates a minimum fill energy of about 10 eV and a second full trench filling energy at about 70 eV. At other range, the filling efficiency becomes worse. In I-PVD a minimum bias voltage must be applied to the ions before their directions can be controlled. According to experiments [156], the necessary bias voltage was about 20 eV. Thus the trench filling simulated at 10 eV should be viewed as an idealistic situation unlikely to be encountered in practice. Similarly, the energy trend at an early stage of filling is less obvious and stands out only when shadowing effects start to become a factor as a deposit builds up at the trench opening.

The reason behind these trends lies in the various effects of the incident energy. At low energy, the incident atoms did not activate reflection or resputtering. Only biased diffusion and athermal rearrangement mechanisms occur. The athermal rearrangement did not play a significant role at the high temperature deposition. The biased diffusion's role was two-fold. It enabled the adatom to diffuse further down inside the trench, it also enabled atoms to relatively easily accumulate at the trench throat area, thus blocking incident atoms from entering the trench inside. This process is responsible for the observed worsening as the energy increased to 20 and then 30 eV. The improvement seen at 50 and 70 eV resulted from the significant activation of both reflection and resputtering. The threshold energies for both processes are about 20 eV. Thus from 20 eV onwards, there are two forces that works against each other. The constructive force on trench filling prevails about 30 eV and maximizes at about 70 eV. With further increasing kinetic energy, the disadvantage of the interactions take over. That is, the reflection and resputtering tends
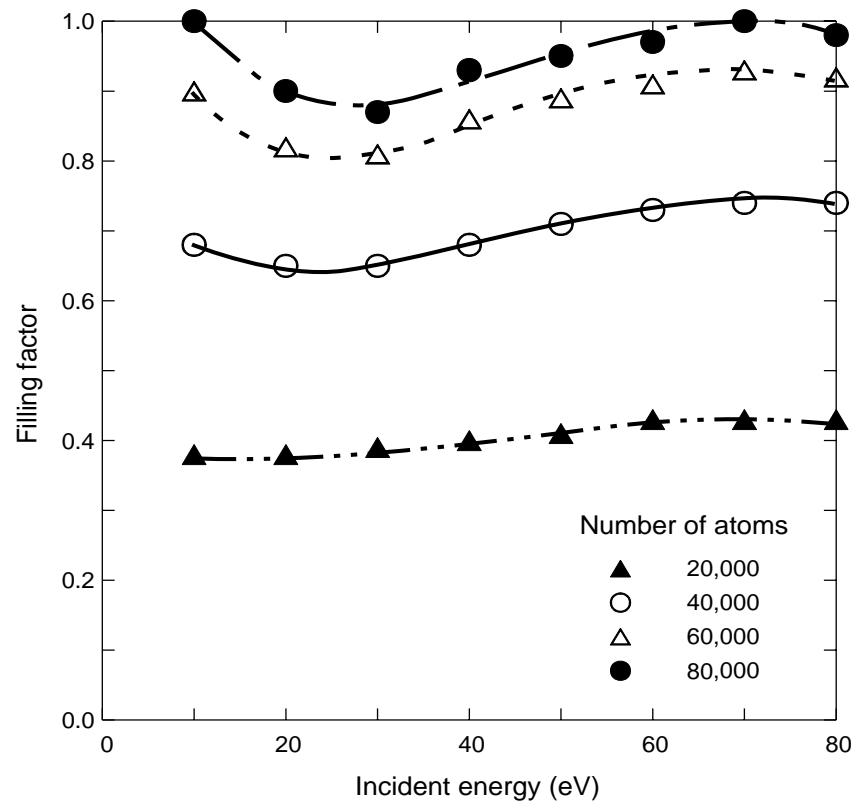
Fig. 9.6. Effect of incidence energy on filling factor. The substrate temperature T = 550 K (T/T_m = 0.48), the deposition rate was 1.0 µm/min, the incidence collimation angle 11° and the aspect ratio of 2. The symbols are used to show the effect of deposition stage on filling factor.

to redistribute the atoms at the upper throat areas and thus speed up overhang formation.

The filling efficiency decreases again.

9.4.3 Effect of substrate temperature and deposition rate

Fig. 9.7 shows the effect of substrate temperature on trench filling under conditions similar to Fig. 9.3. It can be seen that thermal activated diffusion is a must for trench filling process. The intense surface diffusion at high temperature can be seen from the change of mound shape at the trench bottom. At low temperature, Figs. 9.7(a) and (b), the mounds are large. At the complete filling case, Fig. 9.7(d), the mound almost disappears. Intense diffusion helps spread incident atoms to the whole trench bottom. Such intensity also exists on the sidewalls, which ensures an opening trench throat to let flux pass. High

$-11° < \theta < 11°$

0.05 µm

$T/T_m = 0.26$

(a)

$T/T_m = 0.39$

(b)

$T/T_m = 0.43$

(c)

$T/T_m = 0.48$

(d)
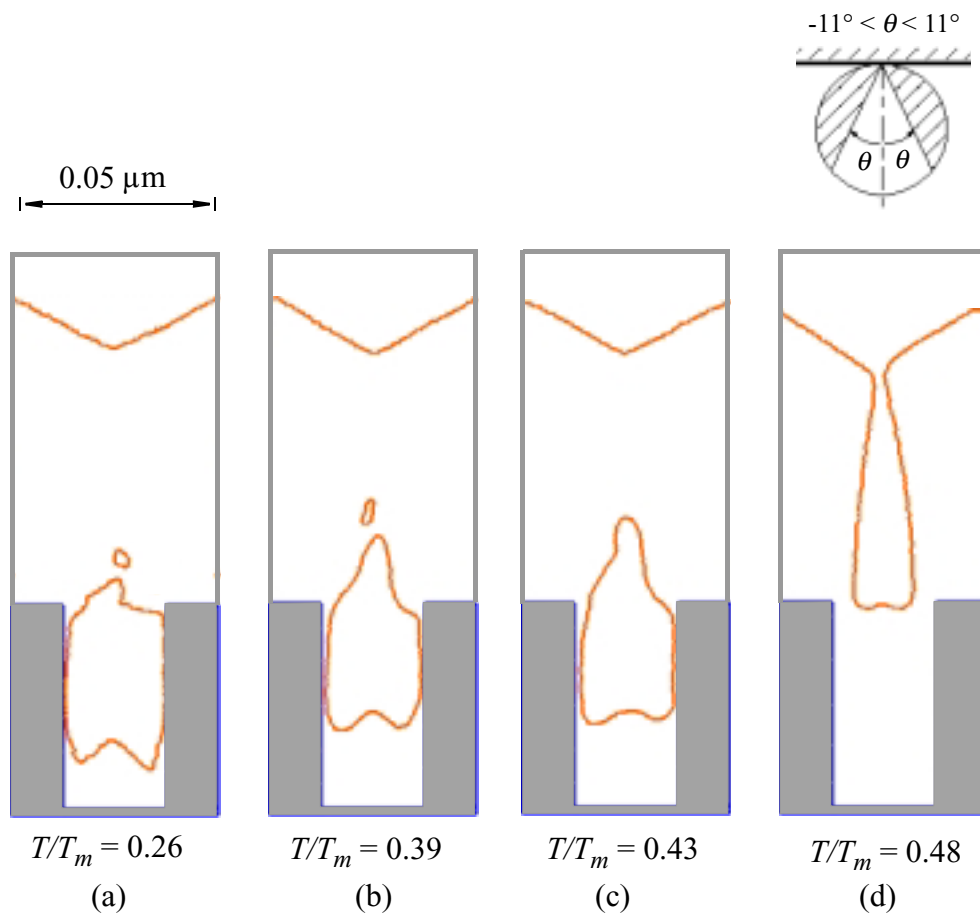
Fig. 9.7. Effect of substrate temperature on trench filling. The incident energy was 50 eV, the incident collimation angle 11°, the deposition rate 1.0 µm/min and the aspect ratio of 2. Nickel atoms of 80000 were used in the simulations.

surface diffusivity at elevated substrate temperature is the basis of the so-called thermal reflow process.

Increasing deposition rate functions similarly to lowing the temperature, Fig. 9.8. Both reduce the chance for adatom relaxation or rearrangement upon arrival at the substrate. The former realizes this by restricting atoms' jumping capability while the latter by reducing available time for atomic jumps. Both conditions prevent the morphology from evolving towards equilibrium

9.4.4 Effect of feature width

To simulate the effect of feature width on trench filling, three considerably different trench widths, 0.05 µm, 0.1 µm and 0.2 µm, have been used. Substrate temperature, deposition rate, incident energy and trench aspect ratio are all kept unchanged at 550 K, 1.0 µm/min, 50 eV and 2.0 respectively. Two sets of collimation angles were used to emphasize the importance of directionality. The number of deposited atoms for the three widths were 80,000, 320,000 and 1,280,000 respectively to ensure the correct square scaling factor for similarity requirement. To better visualize the filling evolution, the surface morphology at three different stages are plotted for each feature. Results for the two arrangements are shown in Figs. 9.9 and 9.10.

Fig. 9.9 is result at θ of 15°. It is evident that the trench filling is more difficult for smaller trench. Fig. 9.10 shows a result at a reduced θ of 11°. It confirms the trend but demonstrates improved coverage. The improvement is seen to result from the enlarged opening at the upper sidewalls.

The reason for the different filling performance at different trench sizes might be tentatively derived from the shape of the inner top surface inside the trench. The difference is best illustrated at 15°. In Fig. 9.9(c), the large trench has developed a convex mound in the centre. The mound becomes very small at the medium trench, Fig. 9.10(b). And it totally disappears in the small one and the inner surface even turns concave.

$-11° < \theta < 11°$

0.05 μm

$R = 1000$ μm/min $R = 100$ μm/min $R = 5$ μm/min $R = 1$ μm/min

(a)   (b)   (c)   (d)
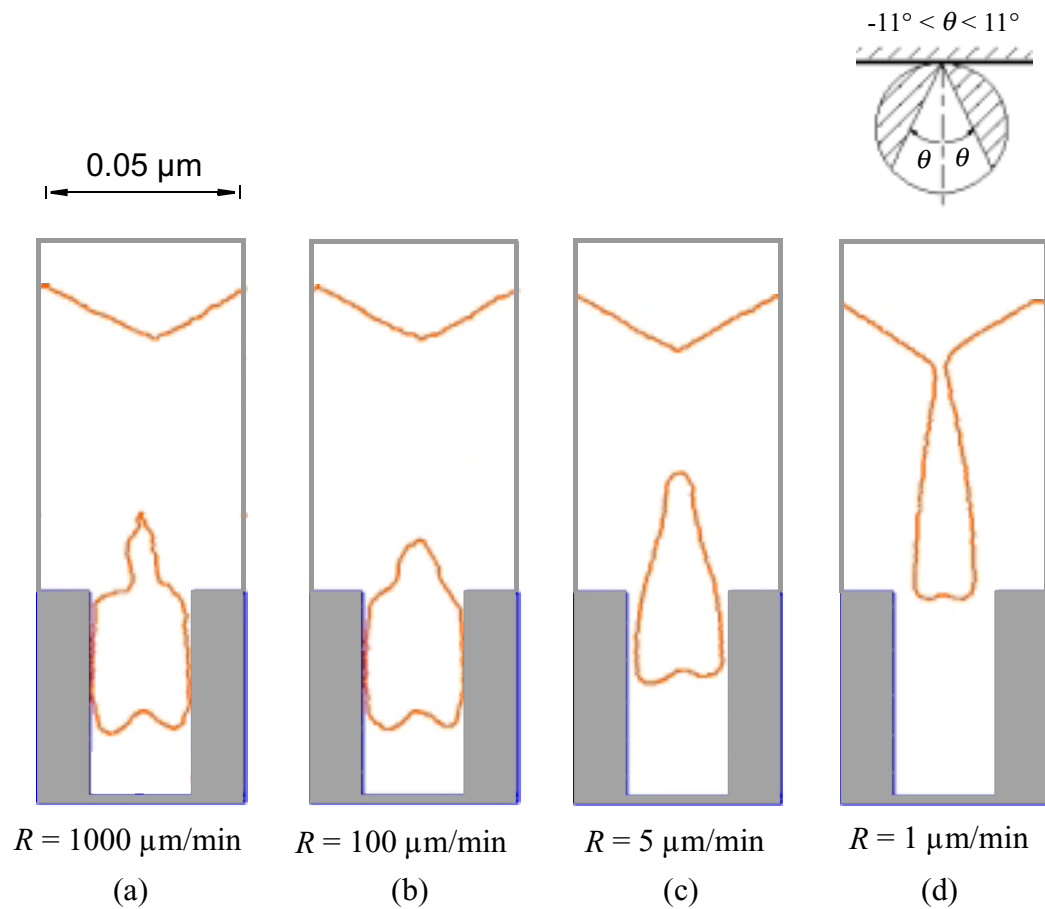
Fig. 9.8. Effect of deposition rate on trench filling. The incident energy was 50 eV, the substrate temperature 550 K (T/T_m = 0.48), the incident collimation angle 11°, the deposition rate 1.0 μm/min and the aspect ratio of 2. Nickel atoms of 80000 were used in the simulations.
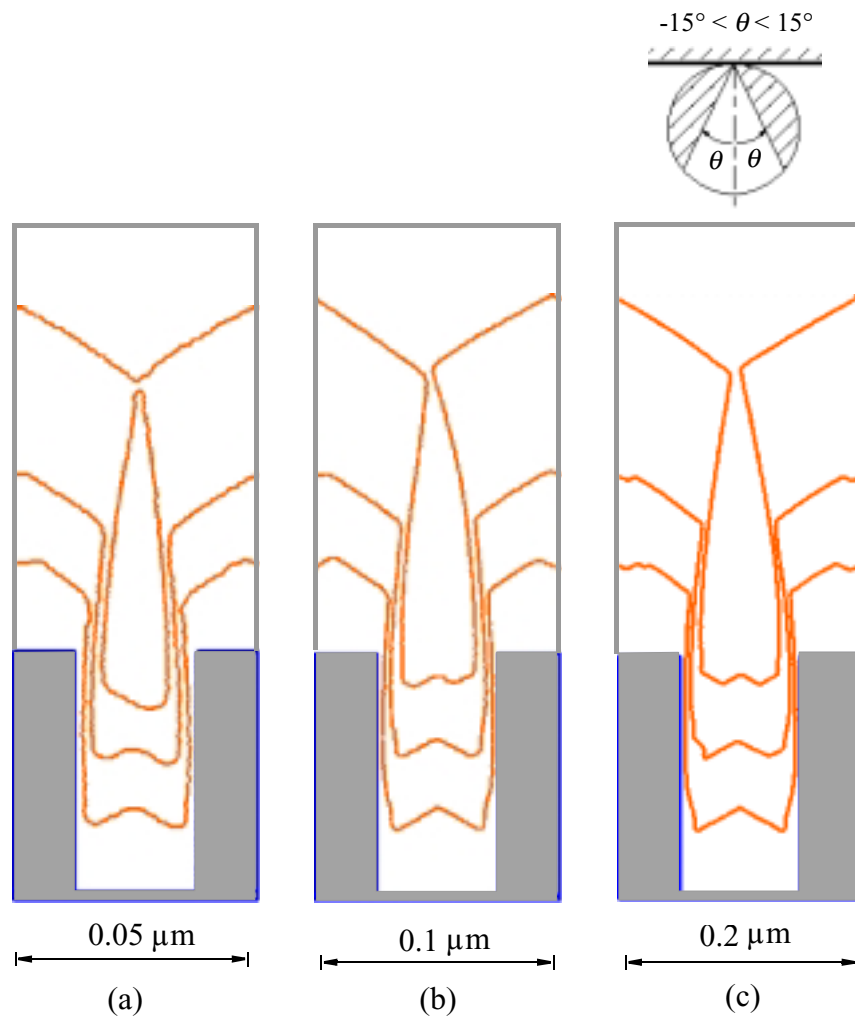
Fig. 9.9. Effect of trench width on filling. The kinetic energy was 50 eV, the deposition rate 1.0 µm/min, the substrate temperature 550 K (T/T_m = 0.48) and the aspect ratio of 2. The incidence collimation angle was fixed at 15°. The number of deposited nickel atoms for the three widths were 80,000, 320,000 and 1,280,000 respectively. Three stages of filling are shown.
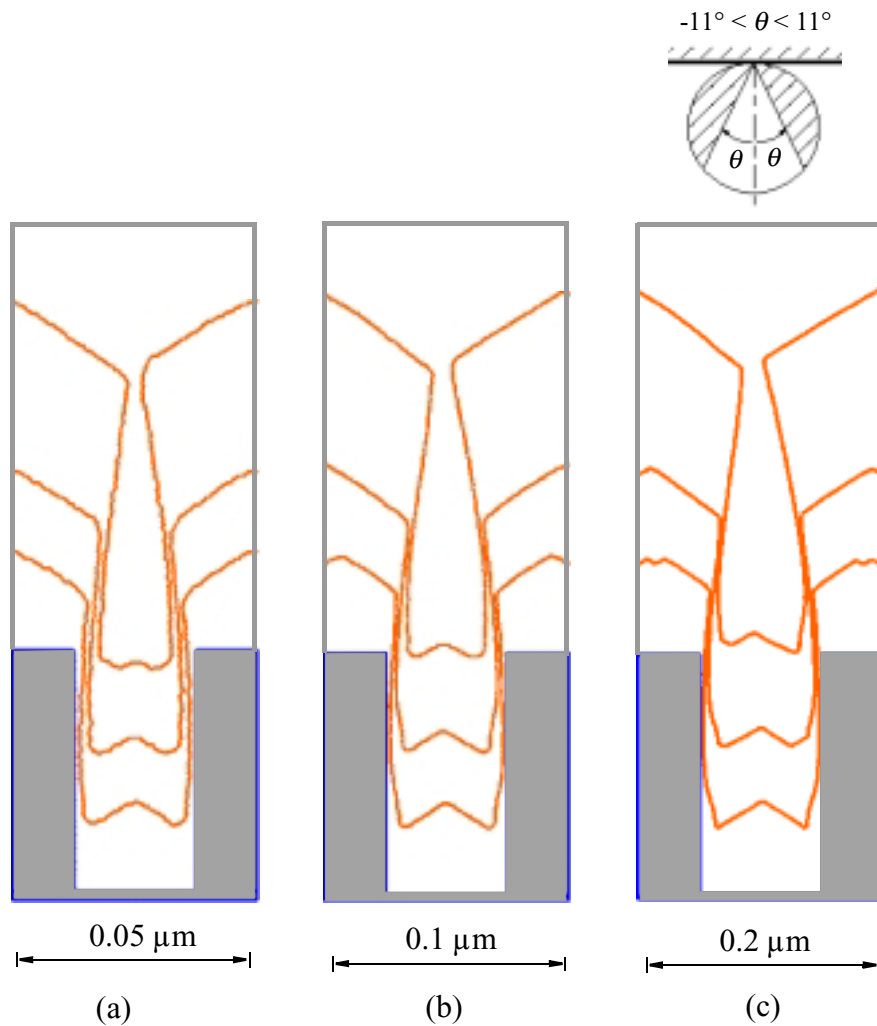
Fig. 9.10. Effect of trench width on filling. The kinetic energy was 50 eV, the deposition rate 1.0 μm/min, the substrate temperature 550 K (T/T_m = 0.48) and the aspect ratio of 2. The incidence collimation angle was fixed at 11°. The number of deposited nickel atoms for the three widths were 80,000, 320,000 and 1,280,000 respectively. Three stages of filling are shown.

Because the process conditions and the geometry are identical, this should be explained as the effect of the length scale on diffusive activities. In the large trench, the incident atoms land mostly in the center (because of the sidewalls' protuberance) and are unable to diffuse away to the distant corners. In contrast, the atoms landing inside the small trench have relatively short distance (small space) and be able to reach the corners. That is, the relative magnitude of distance for mass redistribution decides the end result. In other words, there is an interplay between diffusivity and diffusion space. Mound formation and its relation to diffusion is clearly seen in Fig. 9.7.

The same logic applies to the sidewall because it is the sidewall shape that largely determine the passing of the flux into the inside of the trench. When the trench is small and the distance to the protuberance is short, atoms landing on the sidewalls relatively easily migrate towards the center of the sidewall and block incidence from reaching the inside of the trench.

9.5 Step coverage results

A critical requirement for a liner layer in metallization is continuity. No void should exist on the film, otherwise the metals used to fill the trench can diffuse (during latter high temperature process steps) to reach and destroy active devices. Continuity becomes difficult when deposition is on a large aspect ratio trench because of shadowing from the sidewalls which makes lower sidewall areas difficult to access. One way to overcome the problem is to use directional energetic incident atoms. In this section, the emphasis is on the effect of incident energy on the uniformity of the liner coating. Related effects of trench aspect ratio and collimation extent are also simulated. Again nickel was used for demonstration.

9.5.1 Effect of incident energy

Fig. 9.11 shows a sketch of a commonly observed thin liner coating morphology inside a trench using I-PVD process [1]. The coating on the sidewalls is rather uniform.
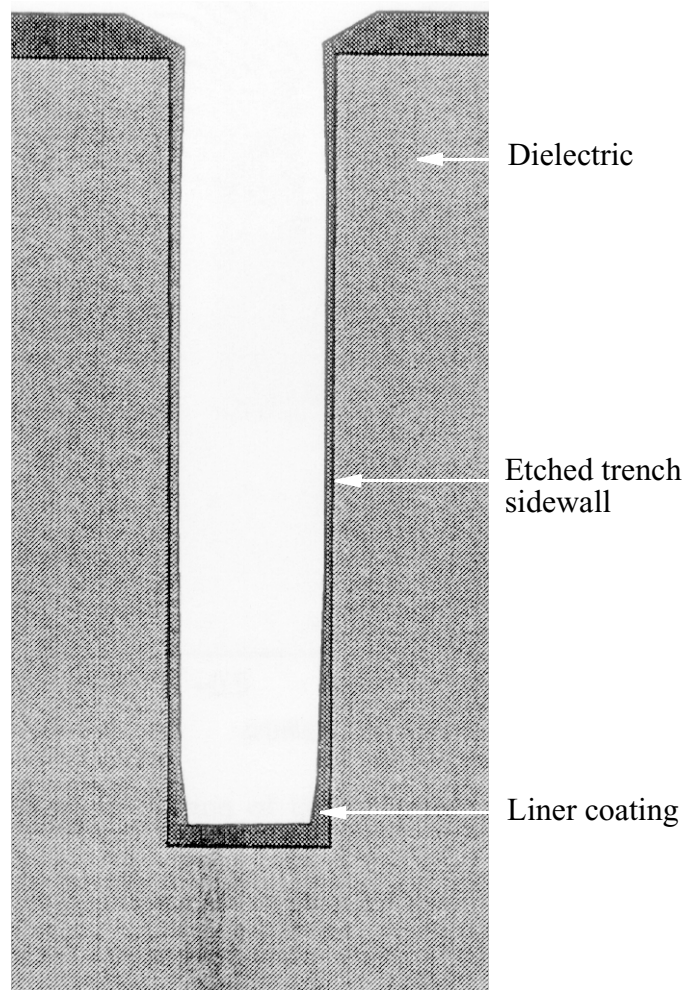
Fig. 9.11. Typical trench liner layer contour using I-PVD process [1, 152]. The lower corner areas have extraordinary thickness because of effect of kinetic energy. This feature can serve as a test if a simulation is correct. The trench has an aspect ratio of 5.

The thickness at the trench throat and the lower corner areas are slightly higher, which makes the coating on the sidewall a concave shape. This concave curve can only be possible when the thickness at the lower corners are bigger than that on the middle section. Since the lower corners are expected to receive the least amount of materials, energy induced material redistribution must account for the unusual thickness.

Fig. 9.12 compares three simulated configurations using different incident energies. When the energy is low (20 eV), Fig. 9.12(a), the lower parts of the sidewalls have insufficient coverage. At higher energy (40 eV), the coverage is evidently improved. When the energy is increased to 70 eV, Fig. 9.12(c), the concave shape seen in Fig. 9.11 can be found. Such energy induced redistribution is caused by the same processes active in trench filling with one caveat. At very high levels of sputtering, the thin liner coating at the trench throat can be completely etched away [12].

9.5.2 Effect of incidence collimation

Fig. 9.13 shows the effect of collimation angle on liner coating process. At 5°, Fig. 9.13(a), most of the sidewalls are sparingly coated because of the narrow incident distribution. But an extraordinary amount of material is seen at the lower corners. Since incident atoms can rarely hit the sidewalls and diffusion would not have a major effect at the low T/T_m of 0.3, the extra deposit must come from the bottom through reflection and resputtering. From the geometry viewpoint, reflection from the bottom should be ruled out, the resputtering thus becomes the only source.

At 25°, Fig. 9.13(b), better sidewall coverage can be seen because of the broader incident distribution. At the same time, the thickness at the bottom is significantly reduced. The reduction in turn decreases the fraction of resputtered atoms that can reach the sidewalls. At 45°, the even broader distribution delivers more atoms onto the upper half of the sidewalls and less onto the lower half and the bottom. The resputtering induced redistribution is even less. An undesired wedge-shape coating thus develops along the

(a) 20 eV   (b) 40 eV   (c) 70 eV
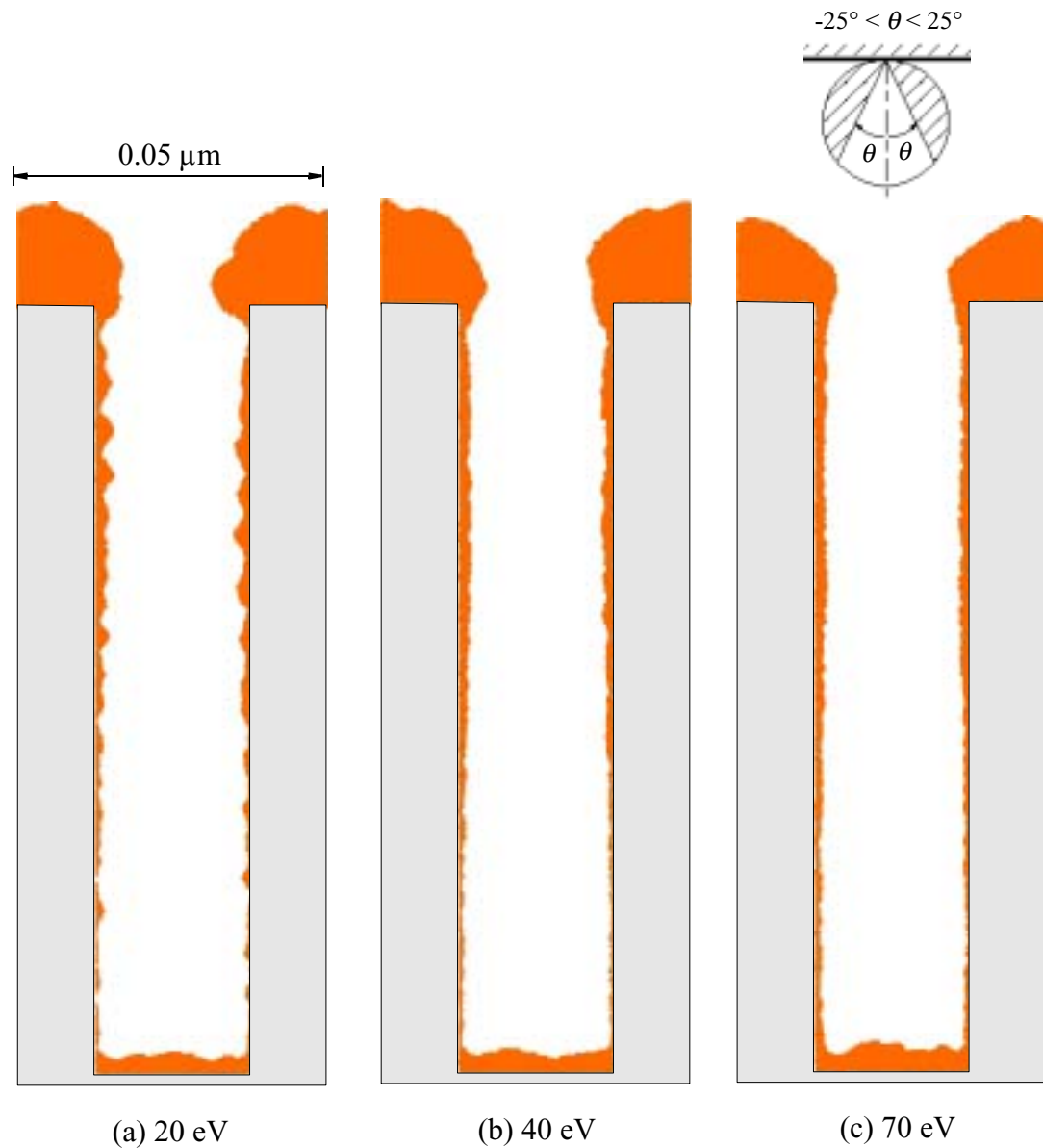
Fig. 9.12. Effect of incident energy on step coverage. The substrate temperature was 350 K ($T/T_m = 0.3$), the deposition rate 1.0 µm/min, the incidence collimation angle 25° and the aspect ratio of 5. 15, 000 nickel atoms were used in the simulations. [Note: The tiny voids seen at the lighter substrate and the darker coating interfaces were artifacts caused by graphics because the substrates were drawn in order to reduce processing time. When the substrates are represented by individual atoms from the simulations, the voids would be filled with atoms from the substrates, a result of interdiffusion].

(a) 5°   (b) 25°   (c) 45°
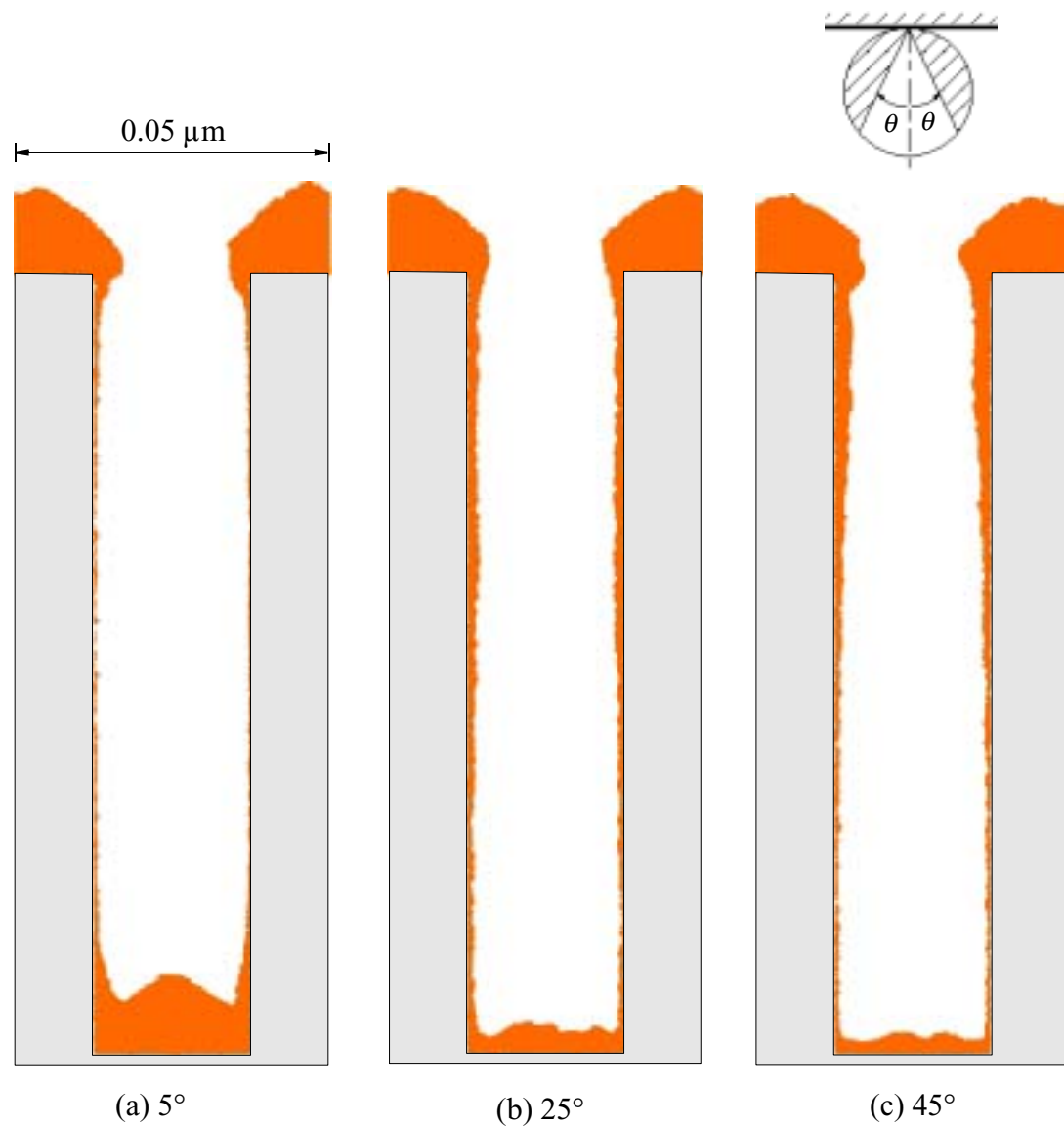
Fig. 9.13. Effect of collimation angle on step coverage. The substrate temperature was 350 K (T/T_m = 0.3), the deposition rate 1.0 μm/min, the incident kinetic energy 70 eV and the aspect ratio of 5. 15, 000 nickel atoms were used in the simulations [see note in Fig. 9.12].

sidewalls. As a result, there exists an optimal incident collimation angle for the liner coating process.

9.5.3 Effect of aspect ratio

Fig. 9.14 shows the aspect ratio effect on liner coating for a fixed set of process conditions. At aspect ratio of 3, the coating thickness along the sidewalls is fairly uniform. At aspect ratio of 5, the coating at the lower half is evidently thinner except for the areas near the corners because of the energy effect. When aspect ratio is increased to 7, undesirable discontinuity can be observed at the lower half in comparison to the configurations seen at aspect ratio of 3 and 5 under the identical conditions. As the resputtering induced redistribution becomes negligible, the corner effect now becomes limited. In such situation, more directional flux is needed to deliver more atoms to the lower half and the bottom on which more redistribution can be induced through resputtering.

9.6 Discussion

In trench metallization, the critical point is to keep the trench throat open as wide as possible during the whole process. Since the throat areas are closer to the source material than the inside, the throat is always the first to receive incident atoms. Since a growing accumulation (of deposit) naturally tends to expand into free space, the trench throat provides an ideal extra space (in addition to the open space above the substrate) for such expansion for deposit adjacent to the throat. These two factors make the deposit at the throat bulge into the space above the trench. The bulging, or protuberance, block subsequent incidence into the inside and further promote the growth of the protuberance. When this process is out of control, a pinch-off (and an internal void) quickly forms. Thus the primary requirement of keeping the throat open is to either avoid its accumulation at the throat or to use some method to rapidly remove it.

There are two ways to aid removal of deposit from the throat area. One is to utilize surface diffusion by increasing substrate temperature. At higher temperature, atoms have

$-25° < \theta < 25°$

0.05 µm

(a) aspect ratio = 3   (b) aspect ratio = 5   (c) aspect ratio = 7
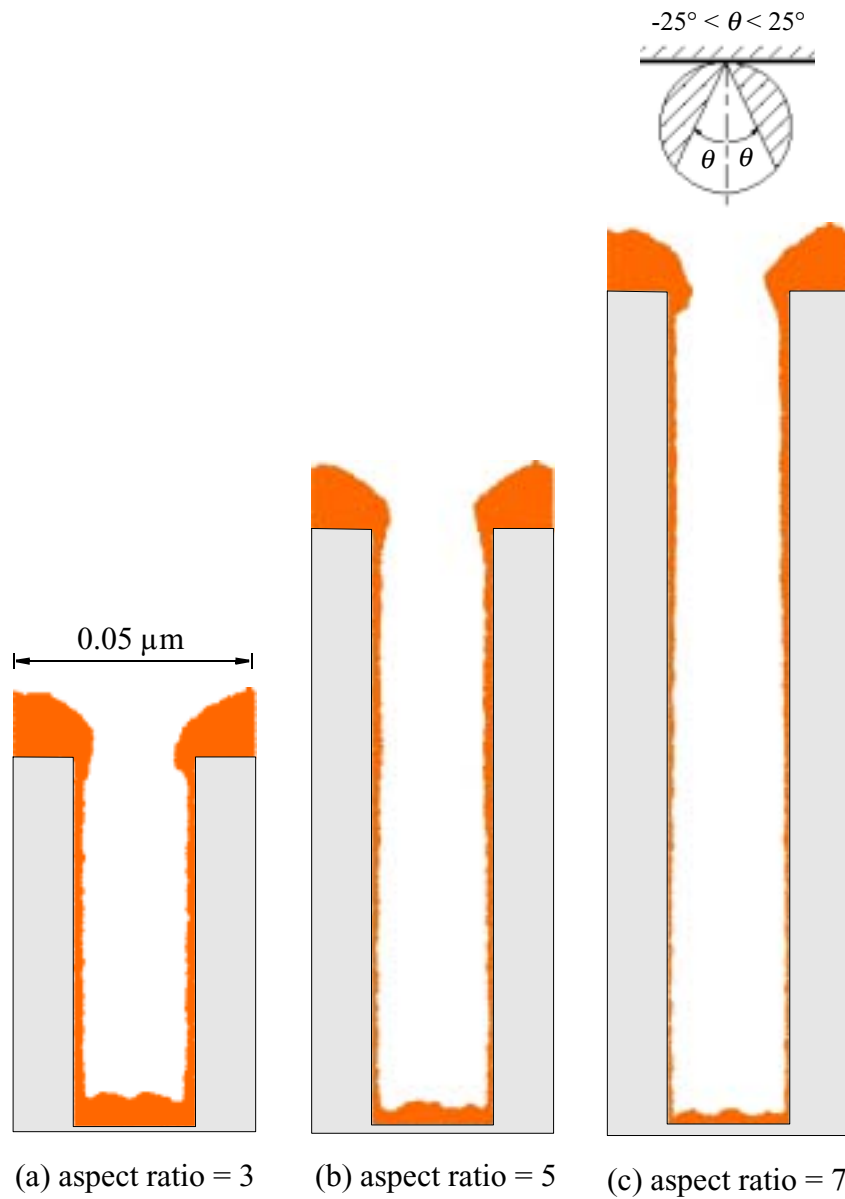
Fig. 9.14. Effect of aspect ratio on step coverage. The substrate temperature was 350 K (T/T_m = 0.3), the deposition rate 1.0 µm/min, the incidence collimation angle 25° and the incident kinetic energy 70 eV. 15, 000 nickel atoms were used in the simulations [see note in Fig. 9.12].

more chance to find stable sites to lower overall system free energy. In other word, when thermal flunctuation is sufficient, surface cusps with small curvature always tends to disappear. This is what the reflow's mechanism comes from. Fig. 9.7 shows only when the substrate temperature reaches certain value that a filling can be completed. However, such a strategy is inappropriate for liner deposition. These materials have very high melting points and to induce surface diffusion requires the use of excessively high temperature.

The second approach is to use energetic bombardment. Energetic atoms can trigger either reflection or resputtering at the impingement site, as described in chapter seven. Either helps redistribute material that otherwise would accumulate at the throat areas. The effect can be seen in Fig. 9.5 where an optimal kinetic energy is needed to achieve the desired effect. When the energy is low, it would not trigger the desired interactions, instead it would induce sometimes harmful athermal biased diffusion that facilitate accumulation at the throat. As is shown in Figs. 9.5(b), (c) and (d), detrimental void tends to form. When the energy is overly supplied, Fig. 9.5(f), energy induced redistributed atoms tend to land and accumulate at the throat areas and make the situation worse. Thus the optimal case is that shown in Fig. 9.5(e). The energetic atoms are able to etch away previous deposited atoms or reflect into the inside of the trench.

Fig. 9.15 shows the experimentally observed effect of kinetic energy [16]. According to the authors, 20 V was about the minimum voltage to effectively pull the ions into the trenches. At that level, the energy induced effects seem to be minimum. Higher voltages induced more resputtering, etc., eventually closing off the feature. The experiments and the simulation were conducted with somewhat different conditions, but the phenomena and the intrinsic mechanisms appear to be similar.

The two discussed above to maintain trench throat openness depend on the process geometry. This establishes the appropriate directional incidence distribution. As shown in Fig. 9.3, a very focused incidence is needed for a complete trench filling. Fig. 9.14 shows
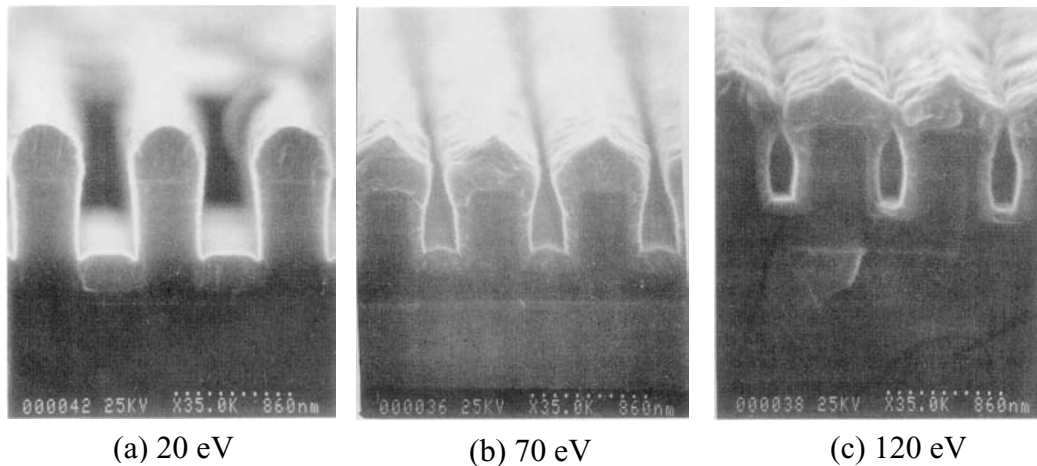
(a) 20 eV   (b) 70 eV   (c) 120 eV

Fig. 9.15. Effect of kinetic energy on trench filling. The AlCu films were deposited into trenches using ionized magnetron sputter deposition as a function of ion energy: (a) 20 eV; (b) 70 eV; (c) 120 eV. The relative ionization in these cases was approximately 50% [16].

a liner deposition under identical process conditions except for aspect ratio. The uniformity of the coating at aspect ratio of 3 is much better than that for aspect ratio of 7. Obviously, adjustments to the flux must be made to achieve the same uniformity as the aspect ratio is varied. Fig. 9.16 shows the observed effect of incidence geometry [16]. Since ionized atoms generally go straight down onto the substrate and neutrals have broad cosine type of distribution, the directionality of the incidence is increased from the left to the right. The low directionality at Fig. 9.16(a) results in an early feature closure while the high directionality leads to a complete fill.

Overall, the two key factors in achieving desired metallization are process geometry and diffusion. Manipulating incident distribution belongs to the geometry domain. Using ionized atoms aim to obtain better directionality. It hence can be said that PVD deposition in metallization is equivalent to a process of interplay of geometry and thermal diffusion. As diffusion generally does not have much room for change under normal process conditions, geometry manipulation becomes more important in reality. This explains all the efforts on using collimator, increasing throw distance and obtaining directionality.

(a) 30%   (b) 50%   (c) 68%
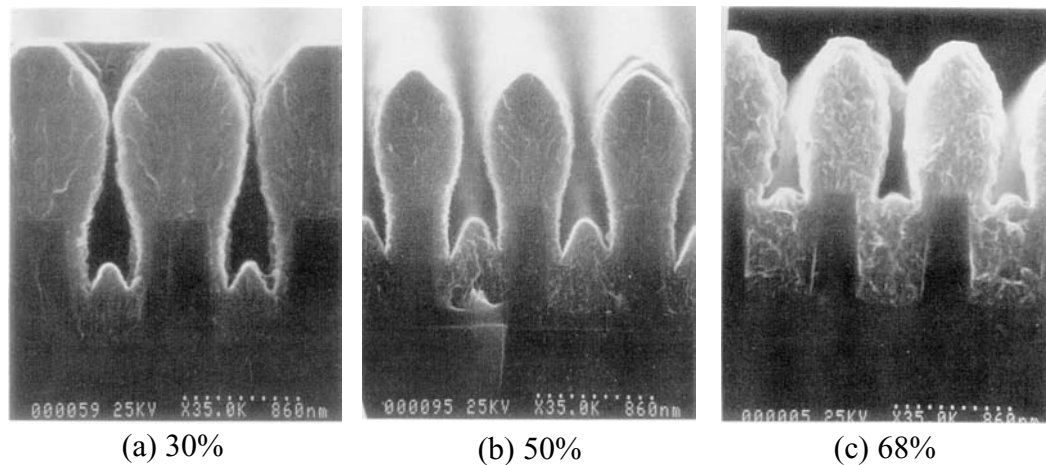
Fig. 9.16. Effect of incidence distribution on trench filling [16]. The AlCu films were deposited into trenches using ionized magnetron sputter deposition as a function of relative ionization at ambient temperature: (a) approx. 30%; (b) approx. 50%; and (c) approx. 68% ionized. The trenches are 4,000 Å in width with aspect ratio of 1.5.

It is interesting to ask how important the post impact atomic assembly processes are to liner deposition. A line-of-sight model can be developed to quantitatively predict the flux illumination of the interior trench. The energy-dependent kMC simulation can then be used to evaluate the role of thermal diffusion and kinetic energy upon coverage.

The basic idea of the illumination model is to obtain a criterion that can be used to characterize the easiness of any point in the trench to access the incident atoms under a given process. The criterion is thus a pure geometry factor and free of any influence of process conditions. In other word, it can be used to identify the intrinsic difficulty of metallization for a feature under the given process geometry.

As is shown in Fig. 9.17, any point on the top surface of the trench is open to the source incidence, thus it has the maximum incidence reach. We define this maximum incidence reach as unity. It is evident that incidence reach for any point inside the trench is less than unity most of the time (except for small aspect ratio feature and normal incidence deposition). A general expression that describes the incidence reach on all of the inside
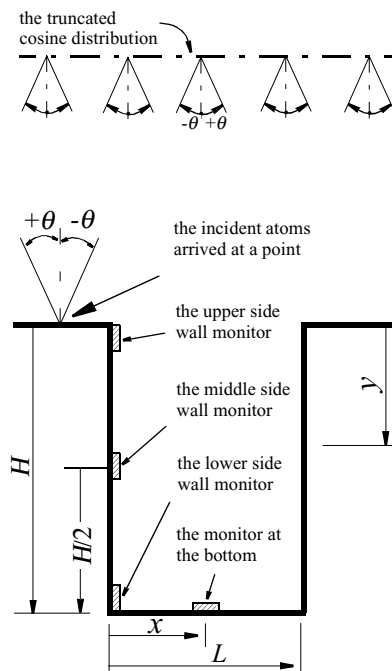
Fig. 9.17. Schematic geometry of trench with parameters for the derivation of flux arrival distributions. Each monitor had a length of *L*/10.

surfaces of the trench, Fig. 9.17, is what we need here. With such expression, we can compare with what we obtain from a real process. We can then identify where are those extra reach (or shortage) come from and what kind of measures we need take to make adjustment. The result is derived in Appendix E.

The curves in Figs. 9.18 and 9.19 are examples of using the expressions derived in Appendix E. Results are plotted by inserting trench size parameters *H* and *L,* an incidence distribution and the various monitoring sites as shown in Fig. 9.17. In order to compare the effect of kinetic energy described presently, the curves in the two figures have the same conditions.

The curves show that flux illumination at the bottom of the trench decreases with increasing cut-off angle. The rate of decrease is particularly steep from 10 to 30°. Illumination of the upper sidewalls increases linearly with increasing the cut-off angle. The
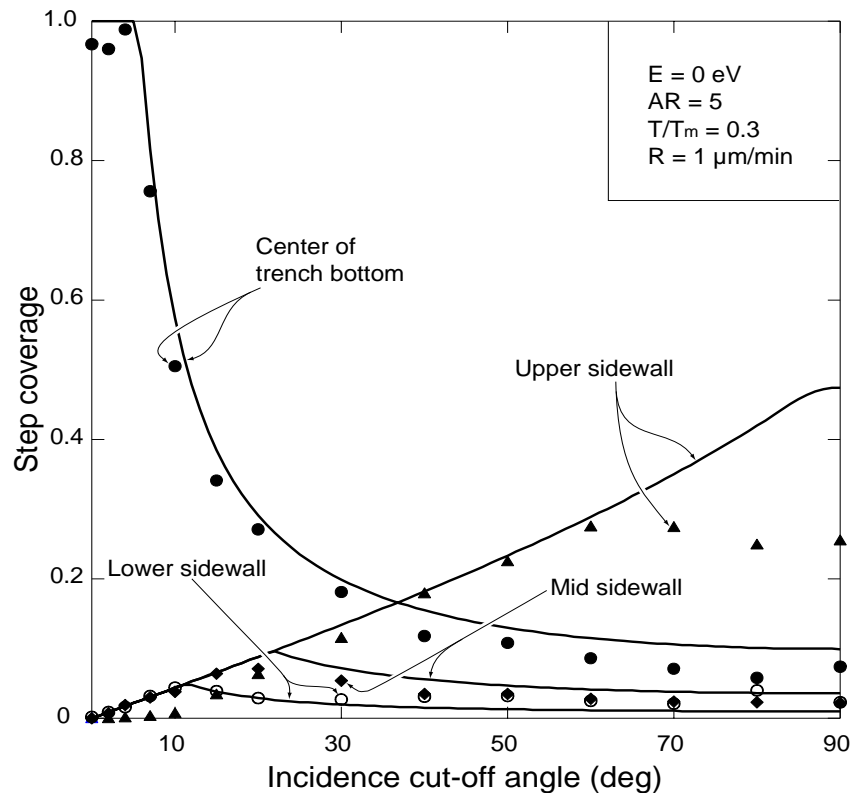
Fig. 9.18. Effect of incident cut-off angle on step coverage. The curve was predicted from the line of sight analysis. The symbols represent simulated data on various positions inside the trench. The simulations were done with temperature of 350 K ($T/T_m = 0.3$), deposition rate of 1.0 μm/min, aspect ratio of 5 and 15000 nickel atoms.

level-off at the end is due to the monitor size. But the reach at the middle and the lower sidewalls have different trends. Both initially increase and then decrease after reaching a maximum. It is interesting to notice that the maximum from the lower sidewall curve identifies a range of cut-off angle (about 0° ~ 12°) that enables a homogeneous flux illumination on the whole sidewalls. Likewise, the maximum from the middle sidewall curve identifies a range of cut-off angle (about 0° ~ 22°) that enables a homogeneous incidence reach on the upper half of the sidewalls. Clearly, with increasing the cut-off angle, the segment with uniform reach would keep shrinking until it completely disappeared at a cut-off angle of 90°. It can be inferred that changing the trench aspect ratio would effect the special segment length as well. It is this type of changing flux illumination along the sidewall

that makes a deposition process for any featured substrate intrinsically difficult. Thus unless very carefully controlled, the upper sidewalls always tend to receive more incident atoms.

To reveal the effect of kinetic energy in mitigating the intrinsic geometry limitation, one simulation with incident energy of 70 eV was compared to another with 0 eV using a trench with aspect ratio of 5. In both cases, nickel was the incidence species, relatively low temperature of 350 K was used to emphasize the effect of energy and the deposition rate was 1.0 µm/min. Both had incidence as a collimated cosine distribution and the same monitoring procedure was set up as in the analysis, Fig. 9.17. Finally, the simulation results were plotted along with the curves in Figs. 9.18 and 9.19 respectively.

Fig. 9.18 shows the points with 0 eV. The data for the simulated bottom coverage follow the curve fairly well. The deviation is rather small for $\theta < 40°$ and becomes appreciable since then. This is caused by the formation of overhang at the upper corners which reduce incidence toward inside. The data for the upper sidewall has agreement only in the medium angle range. The maximum deviation for $\theta > 60°$ comes from pinch-off formation. Significant deviation also occurs at small θ end. This is caused by shadowing, similar to Fig. 9.12(a). The coverage at the middle sidewall follows the analysis fairly well except that the data are consistently lower than the curve. This is due to a general effect of shadowing and the ever-increasing trench aspect ratio because of the constant increase of trench height and decrease of trench width with the deposition. On the contrary, the lower sidewall sees the points mostly above the corresponding curve. This should be an indication of surface diffusion from both the bottom and the wall. Overall, without the effect of kinetic energy, the analysis predicts fairly well the liner thickness inside a trench.

Fig. 9.19 shows the data with 70 eV. Significant differences can be found in comparison to Fig. 9.18. The coverage at the bottom has a similar trend, but points are now mostly above the curve. This is an indication of reflection and resputtering from the side
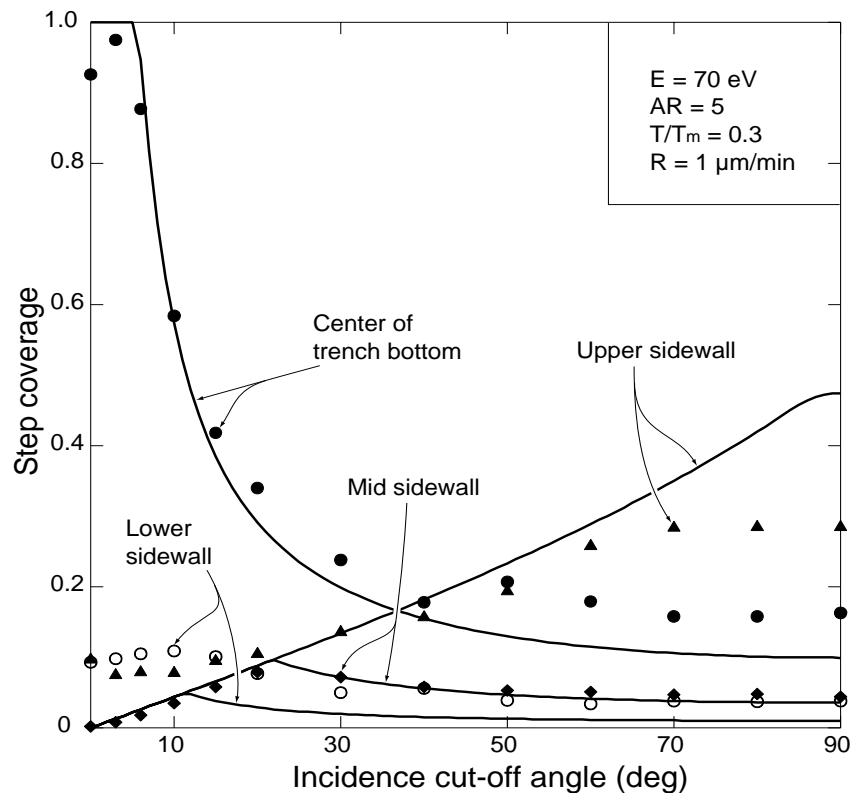
Fig. 9.19. Effect of cut-off angle on step coverage. The curve was predicted from the line of sight analysis. The symbols represent simulated data on various positions inside the trench. The simulations were done with temperature of 350 K ($T/T_m = 0.3$), deposition rate of 1.0 µm/min, aspect ratio of 5 and 15000 nickel atoms.

walls. At the upper walls, a significant difference is seen at the small angle range. The simulated data now are significantly higher than the predicted curve. The reason can be best seen from Fig. 9.12. Severe shadowing seen at low energy, Fig. 9.12(a), is greatly reduced at higher energy because of energetic interactions as in Fig. 9.12(c). The same great difference is also seen at the lower walls. This time, the extra material is due to the resputtering at the bottom, as shown in Fig. 9.13(a). At the middle walls, only overall coverage increase can be seen. Because of its long distance, it neither suffers great loss resulting from shadowing nor it can benefit from the resputtering from the bottom. Therefore, the coverage trends at the three locations under the influence of kinetic energy demonstrate why a concave shape is usually observed for liner coating. Also, the simulated

points in Fig. 9.19 are mostly above the curves, an indication that more than allotted material (by the geometry) has entered the trench [161]. Evidently, the extra material comes from the neighborhood space of the trench and can be discerned in Fig. 9.12.

In summary, the above analysis combined with atomistic simulation can be used to reveal the interplay of process geometry and parameters in achieving a desired metallization performance.

9.7 Conclusions

The energy-dependent kMC simulation was used to explore semiconductor metallization process. The diffusion model, replacing previous diffusion parameter method, was able to realistically simulate the effect of substrate temperature and deposition rate. The impingement incorporating MD derived energy data, replacing practice of sticking coefficient assumption, was able to take into account the constant change of incident kinetic energy and feature locality. The comprehensive approach indicates:

1) There exists an optimal incident kinetic energy for trench filling process. While low kinetic energy induces little resputtering and reflection to redistribute incident atoms into trench inside, high energy causes incident atoms redistribution mostly at the throat areas. At an optimal energy, energy induced athermal diffusion and redistribution are compromised;

2) There is an optimal incidence distribution for metallization process. A pure normal incidence gives the best coverage at the bottom but not enough coverage at the upper sidewall because of shadowing from the throat protuberances. An overly broad distribution tends to concentrate incidence at the trench throat. Only at certain distribution that the coverage at the bottom and the sidewalls can be compromised;

3) The substrate temperature must be high enough to induce surface diffusion for trench filling. Insufficient diffusion tends to accumulate incident atoms at the trench

throat. There is a correlation between temperature and deposition rate. Higher deposition rate reduces available time for atomic relaxation and thus requires higher temperature for compensation;

4) It has been shown that a good process conditions for a big trench may not suitable for a smaller trench with the same aspect ratio;

5) The typical concave shape on sidewalls in liner coating process results form resputtering from the trench bottom. The compensation effect decreases with increasing trench aspect ratio;

6) Combination of a line-of-sight geometrical analysis and an energy kMC simulation can be used to identify a proper process condition.